Anal. Chem. **2010,** *82,* 2237–2242

Positive Frequency Shifts Observed Upon Adsorbing Micron-Sized Solid Objects to a Quartz Crystal Microbalance from the Liquid Phase

Agata Pomorska,[†] Dmitry Shchukin,[‡] Richard Hammond,[§] Matthew A. Cooper,[§,||] Guido Grundmeier,[†] and Diethelm Johannsmann*[,⊥]

Institute of Technical and Macromolecular Chemistry, University of Paderborn, Warburger Str. 100, 33098 Paderborn, Germany, Max Planck Institute of Colloids and Interfaces, Am Mühlenberg 1, 14476 Potsdam-Golm, Germany, Cambridge Medical Innovations, 181 Cambridge Science Park, Cambridge CB4 0GJ, U.K., Institute for Molecular Bioscience, The University of Queensland, St. Lucia, Brisbane, 4072, Australia, and Institute of Physical Chemistry, Clausthal University of Technology, D-38678 Clausthal-Zellerfeld, Germany

By specifically binding derivatized colloidal particles and physisorbing nonderivatized particles to the surface of a quartz crystal microbalance (QCM), we have observed positive shifts of frequency, Δf, in contrast to the negative frequency shifts typically found in adsorption experiments. Evidently, the Sauerbrey relation does not apply to this situation. A comparison of frequencies shifts and bandwidths on different overtones reveals a coupled resonance: at low overtones, Δf is negative, whereas it is positive at high overtones, with maximal resonance bandwidth observed at the crossover point. As predicted by the Dybwad model,[1] the spheres bound to the surface form resonating systems on their own. A composite resonator is formed, consisting of a large crystal with resonance frequency ω and the adsorbed spheres with resonance frequency ω_S. In the case in which the resonance frequency of the small spheres (firmly attached to crystal), ω_S, is higher than the resonance frequency of the crystal, ω, Δf of the composite system is negative (leading to the Sauerbrey limit). In the opposite limit (that is, in the case of large adsorbed particles bound to the sensor surface via a sufficiently weak bridge) Δf is positive. Such a behavior is known from sphere−plate contacts in the dry state. Finite element calculation demonstrates that this phenomena is also plausible in liquid phase media, with Δf critically dependent on the strength of the sphere−plate contact. Operated in this mode, the QCM most likely probes the contact strength, rather than the mass of the particle.

Acoustic resonators are widely used for label-free determination of the interaction between solute molecules and functionalized surfaces.[2] While there is a family of instruments and techniques, the workhorse of the industry at this time is the quartz crystal microbalance (QCM).[3] The QCM consists of a thin plate of a piezoelectric material (usually quartz) that can be electrically excited to oscillate in a thickness shear mode.[4] At the acoustic resonance frequency, both the amplitude of oscillation and the current through the electrodes becomes large. Because the current is large on resonance, the resonance can be easily found with purely electrical instrumentation, in this study by impedance analysis.[5] An important benefit of the QCM is its simplicity, both in operation and in data analysis. When exposed to complex samples (such as colloids), simplicity is a decisive advantage. The crystal surface undergoes a tangential shear motion and the frequency shift is proportional to the area-averaged stress−speed ratio at the crystal surface, however complex the sample may be.[4]

For small molecules, the sensor response typically is described by the Sauerbrey equation[6]

$$\frac{\Delta f^*}{f_F} = -\frac{2f}{Z_q} m_f \qquad (1)$$

where $\Delta f^* = \Delta f + i\Delta\Gamma$ is the complex frequency shift, Γ is the half-bandwidth at half-maximum, f_F is the frequency of the fundamental, f is the resonance frequency, $Z_q = 8.8 \times 10^6$ kg m^{-2} s^{-1} is the acoustic impedance of AT-cut quartz, and m_f is the mass per unit area of the deposited material. Equation 1 makes use of the complex frequency shift for reasons of consistency with the equations shown further below. For the Sauerbrey case, the frequency shift is purely real. There no shift in the bandwidth. Many researchers use dissipation, $D = 2\Gamma/f$, rather than bandwidth to quantify dissipative processes.[7] Dissipation and bandwidth are completely equivalent.

Due to the sharpness of the resonance, the QCM easily reaches monolayer sensitivity. However, monolayer sensitivity often is insuf-

* To whom correspondence should be addressed. E-mail: johannsmann@pc.tu-clausthal.de.
[†] University of Paderborn.
[‡] Max Planck Institute of Colloids and Interfaces.
[§] Cambridge Medical Innovations.
[||] The University of Queensland.
[⊥] Clausthal University of Technology.

(1) Dybwad, G. L. *J. Appl. Phys.* **1985**, *58*, 2789.
(2) Cooper, M. A. (Ed.) *Label-Free Biosensors: Techniques and Applications*; Cambridge University Press: New York, 2009.
(3) Steinem, C.; Janshoff, A. (Eds.) *Piezoeletric Sensors*; Springer: New York, 2006.
(4) Johannsmann, D. *Phys. Chem. Chem. Phys.* **2008**, *10*, 4516.
(5) Beck, R.; Pittermann, U.; Weil, K. G. *Ber. Bunsen-Ges. Phys. Chem.* **1988**, *92*, 1363.
(6) Sauerbrey, G. *Z. Phys.* **1959**, *155*, 206.
(7) Rodahl, M.; Kasemo, B. *Rev. Sci. Instrum.* **1996**, *67*, 3238.

10.1021/ac902012e
Published on Web 02/18/2010

ficient for studying the affinity of certain target molecules to surfaces. Depending on the concentration of the analyte and the lateral density of receptors, the degree of coverage may be deep in the submonolayer regime. Also, the binding kinetics may contain valuable information,[8] such as the kinetic constants k_{on} and k_{off}, hence submonolayer sensitivity is needed. Submonolayer sensitivity can be achieved with the QCM, but there remains a disadvantage of the QCM compared to competing optical techniques.[9] For example, surface plasmon resonance (SPR) spectroscopy typically has a detection limit in the range of well below 1 pg/mm,[2,9] which is difficult to reach with the QCM.

One natural way of amplifying the signal consists of attaching the target molecules to larger objects (such as bulky molecules or small colloidal spheres), which are more efficiently detected than the target molecules itself.[10] This approach has, for instance, been demonstrated to enhance the signal observed for DNA hybridization using DNA-conjugated nanoparticles captured by surface-bound single-stranded templates.[11−20] In a similar manner, sensitive protein detection can be achieved by employing antibody-coated colloids in an sandwich immunoassay for biomarkers such as C-reactive protein.[21] In these cases, small (15−100 nm diameter) gold nanoparticles were used. When we performed similar experiment with larger diameter particles, we have repeatedly encountered *positive* frequency shifts upon adsorption. A positive Δf is incompatible with both the Sauerbrey equation (which applies to thin rigid films) and the Kanazawa equation (applicable to semi-infinite viscoelastic media). Even viscoelastic films usually lead to negative frequency shifts. Within all these models the effective mass of the resonator increases, thereby slowing down its movement. It is hard to see how added mass should speed up the oscillation.

As has been pointed out by Dybwad,[1] positive frequency shifts occur when the crystal is put into contact with a sufficiently large sphere. Such experiments have been carried out numerous times in the dry state.[22−25] The frequency shift is positive because the effective *stiffness* of the composite resonator increases, rather than its mass. If the sphere is connected to the crystal via a small bridge (a "point contact"), the forces exerted by the crystal do not actually move the sphere around in space. The sphere is "clamped" by inertia. However, since the sphere is connected to the crystal, it does exert a restoring force if the crystal is tangentially displaced. This restoring force adds

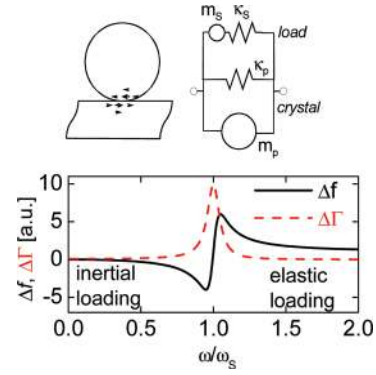

Figure 1. (Top left) Sketch of a sphere adsorbed to the surface of a quartz crystal microbalance. The sphere and the contact between the sphere and the surface constitute a resonating system of their own. (Top right) Mechanical representation. The crystal and the sample form a system of coupled resonators with two resonance frequencies $\omega_s = \sqrt{(\kappa_p/m_p)}$ (crystal) and $\omega_s = \sqrt{(\kappa_s/m_s)}$ (sphere). The frequency shift of the composite resonator relative to the unloaded crystal depends on whether ω_S is higher or lower than ω. ω_S is high for small particles tightly attached to the crystal, which leads to Sauerbrey-type behavior ("inertial loading"). In the opposite limit, the sphere remains immobile in space due to inertia, but exerts a restoring force onto the crystal, thereby increasing the stiffness of the composite resonator ("elastic loading"). The bottom shows the solution to eq 2.

to the internal stiffness of the crystal and thereby speeds up the oscillation.

Dybwad has put this model (termed "coupled-resonance model" in the following) into quantitative terms.[1,26] He concludes that the sphere in contact with the plate forms a second resonator with its own resonance frequency, ω_S. The sketch at the top of Figure 1 shows the geometry and a mechanical representation. For a small mass tightly attached to the crystal, ω_S is much larger than the resonance frequency of the crystal, ω. Such a situation is, for instance, encountered with individual molecules physisorbed to the crystal surface.[27] Working through the algebra, one finds the Sauerbrey equation recovered from the coupled-resonance model if $\omega_S \gg \omega$. This situation is termed "inertial loading" in Figure 1. Δf is negative as long as the adsorbed objects are small enough. However, for large (micrometer-sized) spheres attached to the crystal via weak bridges, ω_S, may be *smaller* than ω. In this limit, one arrives at a positive Δf, proportional to the stiffness of the contact and independent of the sphere's mass. This situation is termed "elastic loading" in Figure 1.

More quantitatively, the coupled-resonance model predicts[1,24,28]

$$\frac{\Delta f + i\Delta\Gamma}{f_F} = \frac{N_S m_S \omega}{\pi Z_q} \frac{(\omega_S^2 + i\omega\gamma)}{(\omega^2 - \omega_S^2 - i\omega\gamma)} = \frac{-N_S m_S \omega}{\pi Z_q} \frac{1}{1 - \dfrac{\omega^2}{\omega_S^2 + i\omega\gamma}} \approx \frac{-N_S m_S \omega}{\pi Z_q} \frac{1}{1 - \dfrac{\omega^2}{\omega_S^2}} \quad (2)$$

N_S is the number density of the spheres. The resonance frequency of the sphere−plate system was also considered to

(8) McDonnell, J. M. *Curr. Opin. Chem. Biol.* **2001**, *5*, 572.
(9) Homola, J. *Anal. Bioanal. Chem.* **2003**, *377*, 528.
(10) Welsch, W.; Klein, C.; vonSchickfus, M.; Hunklinger, S. *Anal. Chem.* **1996**, *68*, 2000.
(11) Tao, L.; Ji'an, T.; Han, M. M.; Jiang, L. *Chin. Sci. Bull.* **2003**, *48*, 873.
(12) Liu, T.; Tang, J.; Jiang, L. *Biochem. Biophys. Res. Commun.* **2004**, *313*, 3.
(13) Weizmann, Y.; Patolsky, F.; Willner, I. *Analyst* **2001**, *126*, 1502–1504.
(14) Liu, T.; Tang, J.; Jiang, L. *Biochem. Biophys. Res. Commun.* **2002**, *295*, 14.
(15) Willner, I.; Patolsky, F.; Weizmann, Y.; Willner, B. *Talanta* **2002**, *56*, 847.
(16) Weizmann, Y.; Patolsky, F.; Willner, I. *Analyst* **2001**, *126*, 1502.
(17) Ha, T. H.; Kim, S.; Lim, G.; Kim, K. *Biosens. Bioelectron.* **2004**, *20*, 378.
(18) He, F. J.; Liu, S. Q. *Talanta* **2004**, *62*, 271.
(19) Zhao, H. Q.; Lin, L.; Tang, J.; Duan, M. X.; Jiang, L. *Chin. Sci. Bull.* **2001**, *46*, 1074.
(20) Fritzsche, W.; Taton, T. A. *Nanotechnology* **2003**, *14*, R63.
(21) McBride, J. D.; Cooper, M. A. *Nanobiotechnology* **2008**, *6*, 5.
(22) Laschitsch, A.; Johannsmann, D. *J. Appl. Phys.* **1999**, *85*, 3759.
(23) Berg, S.; Johannsmann, D. *Phys. Rev. Lett.* **2003**, *91*, 145505.
(24) D'Amour, J. N.; Stålgren, J. J. R.; Kanazawa, K. K.; Frank, C. W.; Rodahl, M.; Johannsmann, D. *Phys. Rev. Lett.* **2006**, *96*, 058301.
(25) Zhang, Q. L.; Lec, R. M.; Pourrezaei, K. *IEEE Trans. Ultrason. Ferroelectr. Freq. Control* **2006**, *53*, 167.
(26) A derivation using the variables employed here is given: Du, B. Y.; Konig, A. M.; Johannsmann, D. *New J. Phys.* **2008**, *10*, 053014.
(27) The detailed calculation shows that gold nanoparticles with a size below 100 nm also behave as small in this sense.
(28) Actually, eq 2 is algebraically different from Dybwad's original result. Dybwad's result is more complicated, but in essence the same.

be complex, where the imaginary part was termed $\omega\gamma$. γ quantifies dissipative components of the sphere−plate interaction. The bottom part of Figure 1 shows the solution to eq 2. Further insight is obtained from Taylor expansions for large and small ω. For $\omega \ll \omega_S$, one finds

$$\frac{\Delta f + i\Delta\Gamma}{f_F} \approx \frac{-N_S m_S \omega}{\pi Z_q} \frac{1}{1 - \frac{\omega^2}{\omega_S^2}} \approx \frac{-N_S m_S \omega}{\pi Z_q} = \frac{-2fN_S m_S}{Z_q} \tag{3}$$

that is the Sauerbrey equation with $N_S m_S$ inserted for the mass per unit area. In the opposite limit of $\omega \gg \omega_S$, one finds

$$\frac{\Delta f + i\Delta\Gamma}{f_F} \approx \frac{-N_S m_S \omega}{\pi Z_q} \frac{1}{1 - \frac{\omega^2}{\omega_S^2}} \approx \frac{N_S m_S \omega_S^2}{\pi Z_q \omega} = \frac{1}{\pi Z_q} \frac{N_S \kappa_S}{\omega} \tag{4}$$

The last identity on the right-hand side made use of $\omega_S = (\kappa_S/m_S)^{1/2}$, where κ_S is the stiffness of the sphere−plate contact. Clearly, the frequency shift is positive, it is proportional to the stiffness of the contact, and it scales inversely with ω, that is, it scales inversely with overtone order n.

Note, however, that the above consideration apply to spheres *in the dry state*. Whether or not a similar situation can occur in liquids is not easily addressed. First, spheres in liquids are moved around by the liquid if they are located inside the evanescent acoustic wave. Second, the liquid in between the sphere and the plate strongly contributes to the sphere−plate interaction, making any link rather strong. The liquid transports a substantial amount of stress across the gap both because of the high frequency. Viscous stress is proportional the product of viscosity and frequency. Also there are gradients in hydrostatic pressure generated by the movement of the particles. Simple-minded diagrams such the one shown on the upper right in Figure 1 do not apply in a liquid environment.

Below we report on two examples for positive frequency shifts occurring for colloidal adsorbates. The first example concerned aggregates of mesoporous nanocontainers (NCs). The potential applications of these objects are wide-ranging and outside the scope of this work. The finding of a positive frequency shift was serendipitous and is per se not related to the application. In the experiment on the nanocontainers, we employed an instrument that determines frequency shifts as well as bandwidths and does so on a number of different overtones. For a simple Sauerbrey situation, these data would be redundant. However, for the question of whether or not the coupled-resonance model applies, the comparison of data from different harmonics is key to the answer. The comparison shows that the coupled-resonance model can indeed explain the positive Δf. The particular sample investigated here (nanocontainers; see Figure 2) is rather complicated. The particles are not spheres. Importantly, the occurrence of a coupled resonance is by no means limited to spheres. The coupled resonance requires a large object linked to the sensor surface via a weak link. The shape of the object only comes into play when detailed quantitative predictions are desired.

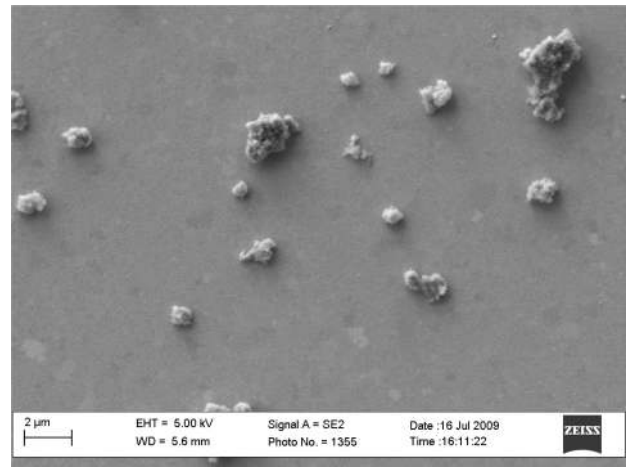

Figure 2. SEM micrograph of the colloidal aggregates used in the first set of experiments (Figures 3 and 4). This specific sample consisted of PSS-terminated TiO_2 nanocontainers on a gold substrate functionalized with an aminothiol SAM.

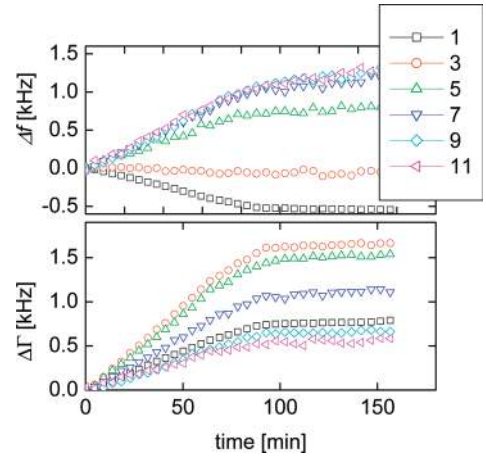

Figure 3. Raw QCM data on adsorption of PSS-terminated NCs on SAM of aminothiol (positively charged). The top and the bottom show shifts of frequency and bandwidth in the course of an adsorption experiments, respectively. The magnitude of all quantities steadily increases with time, until the adsorption was stopped at $t = 90$ min. However, the magnitude and sign of Δf depends on the overtone order, as indicated in the legend.

The second example concerns magnetic colloids. These were employed both for the purpose of signal amplification and for speeding up the transport between the bulk and the sensing surface by magnetic fields. In this case, the instrument at hand only provided the frequency shift on one single harmonic (which was the fundamental). Therefore, the proof that the positive Δf indeed goes back to point contacts (and a concomitant coupled resonance) is less straightforward than in the first example. Nevertheless, the second example is important because it highlights the importance that point contacts may have in the context of protein interaction analysis and the study of specific interactions.

MATERIALS AND EXPERIMENTAL PROCEDURES

Inorganic Nanocontainers. Details of the properties of these nanocontainers and their intended use are unessential in this context. Details will be published in a later publication.[29] Briefly,

(29) Pomorska, A.; Shchukin, D.; Grundmeier, G.; In preparation.

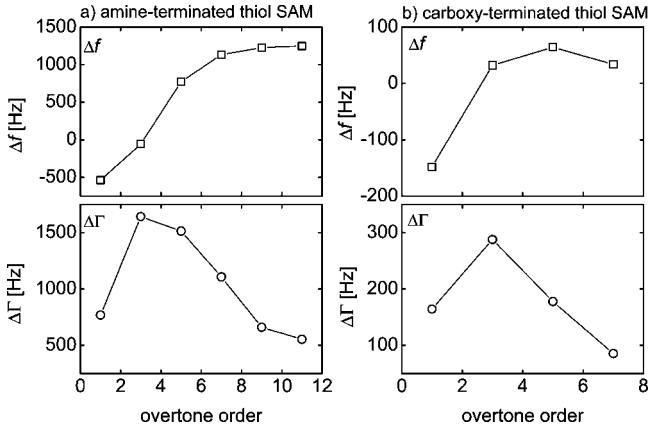

Figure 4. (a) Time-averaged values of Δf and $\Delta\Gamma$ from Figure 3 for $t > 90$ min (stationary state after end of the adsorption experiments). There is a coupled resonance. Δf changes sign at $n = 3$ and the dissipation as quantified by the shift in bandwidth, $\Delta\Gamma$, goes through a maximum at this overtone order. (b) A second example of a coupled resonance for a different material (raw data not shown). In the case shown in panel a, the surface was positively charged by employing an amine-terminated thiol self-assembled monolayer (SAM). The spheres were negatively charged. In the second case (panel b), the charging was reversed. Otherwise, the materials were similar.

the mesoporous TiO_2 particles ("nanocontainers", NCs) were coated with polyelectrolyte multilayers according to the layer-by-layer technique.[30] Polyallylamine hydrochloride (PAH) and polysodium 4-styrenesulfonate (PSS) were used as polycations and polyanions, respectively. PSS- and PAH-terminated particles are negatively and positively charged, respectively. The NCs were adsorbed on to the gold electrode of AT-cut quartz crystals (5 MHz fundamental, Filtech). Prior to deposition, the surface was functionalized with a self-assembled monolayer (SAM) of amine-terminated (positively charged) or carboxy-terminated thiols (negatively charged). At suitable pH values, amine- and carboxy-terminated surfaces carry positive and negative charge, respectively. The charge on the NCs and the surface was always opposite, providing for electrostatic attraction.

The following experimental steps were undertaken. First, the gold electrodes were coated with the SAM. Each surface was examined by means of polarization-modulated infrared reflection absorption spectroscopy (PM-IRRAS), thereby proving the success of the self-assembly process. The presence of a suitably charged SAM is needed in order to adsorb the containers. The adsorption experiments were performed by pumping a dispersion of the NCs in water (0.06 g/L) through the QCM chamber. A baseline in pure water was acquired before each experiment. After injection, the bandwidth always increased. The frequency shift, on the contrary, either increased or decreased, depending on the overtone order. After about 1 h, the adsorption process was stopped by purging with pure water. After the adsorption was stopped, a stationary state was reached for all overtones. Subsequently, the samples were examined by scanning electron microscopy (SEM, field emission electron gun scanning electron microscope Zeiss Neon 40) to reveal the adsorption and the distribution of containers on the surface. Importantly, the NCs at hand always *aggregated* into larger units. Figure 2 shows an SEM image. The aggregates had a size in the micrometer range, which is a prerequisite for the occurrence of positive Δf.

Functionalized Magnetic Nanoparticles. Two diameters of magnetic particle were used, both of which showed positive frequency changes when the particles were bound to the QCM sensor surface. In the first experiment, 2.8 μm diameter streptavidin-coated beads were used (Dynabead M280 Streptavidin). In the second experiment, 1.0 μm diameter streptavidin-coated beads were used (Dynabead MyOne Streptavidin). All experiments were carried out under PBS buffer on a 16.5 MHz fundamental AT-cut quartz crystal QCM (AKtiv cassette supplied by TTP LabTech Ltd.). This cassette has two QCM sensors on a single piece of crystal with associated sample flow cells, fluid connections, and electrical connections, thus providing control and measurement sensors in a single cassette. The immobilization of proteins to the sensor surface was carried out using a RAPid4 instrument (TTP LabTech Ltd.). The wet sensor cassette was then inserted into an in-house bespoke test rig for addition of magnetic particles. The test rig consisted of a fluidic system for passing liquid across the sensor surfaces, a microscope for observing the sensor surface, a pair of permanent magnets for attracting the magnetic particles to the sensor surface, and drive electronics to excite the QCM. The drive electronics was a simple self-oscillator circuit optimized to drive the QCM at its fundamental resonant frequency. The circuit included a switch so each sensor in the cassette is excited in turn, thus eliminating cross-talk between the sensors. The fundamental frequency of resonance of the circuit is measured using a frequency counter, and this is connected to in-house software to sample and log the data.

In the assay, a polyclonal mouse IgG antibody (Jackson Immunologicals, 50 μg/mL) was immobilized to the sensor surface followed by a biotinylated antimouse antibody (Sigma, 5 μg/mL) in the measurement channel and a nonbiotinylated antimouse antibody (Sigma, 5 μg/mL) in the control channel. Sensor surfaces (that present a carboxylic acid functionality to the solution phase) were activated with a 1:1 mixture of 400 mmol/L 1-ethyl-3-[3-dimethylaminopropyl]carbodiimide hydrochloride (EDC) and 100 mmol/L *N*-hydroxysuccinimide (NHS; both from Perbio Science UK Ltd., Cramlington, UK), prepared in 0.22 μm-filtered deionized water and mixed immediately prior to use (final concentrations; 200 mmol/L EDC and 50 mmol/L NHS). EDC−NHS was injected simultaneously across both sensor surfaces for 3 min. Affinity-purified rabbit antimouse-Fc (Stratech Scientific Ltd./Jackson ImmunoResearch, Soham, UK), mouse IgG, and biotinylated mouse IgG (Stratech/Jackson) were prepared for immobilization at 50 μg/mL in z buffer comprising 10 mmol/L sodium acetate, pH 4.5, and were injected simultaneously across separate sensor surfaces for 3 min. Nonreacted NHS esters were then capped with 1 mol/L ethanolamine (Sigma-Aldrich, Poole, UK) prepared in 0.22 μm filtered deionized water, pH 8.5. Running buffer between sample injections was Dulbecco's modified phosphate buffered saline (PBS; Sigma-Aldrich, Poole, UK), at a flow rate of 50 μL/min. Finally, the 2.8 or 1.0 μm diameter streptavidin-coated magnetic particles (Dynal) were pumped through both flow cells; the flow rate and concentration of particles was varied from experiment to experiment.

(30) Decher, G. *Science* **1997**, *277*, 1232.

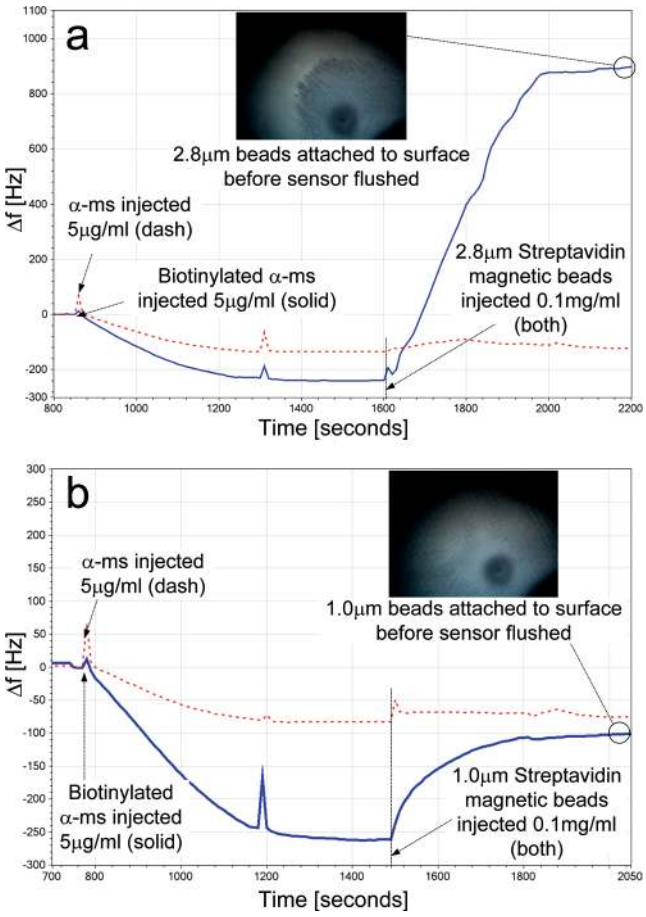

Figure 5. (a) Logged frequency shift Δf data for binding of 2.8 μm diameter streptavidin-coated magnetic particles. Note the decrease in frequency as antibodies bind on both channels (as expected for small molecules binding to a QCM surface) and the following increase in frequency as the large magnetic particles are adsorbed to the surface. The inset photograph shows the sensor surface before flushing. (b) Logged frequency shift Δf data for 1.0 μm diameter streptavidin-coated magnetic particles. Note the same decrease in frequency as the antibodies bind and the increase in frequency with bead adsorption. Again, the inset photograph shows the sensor surface before flushing.

RESULTS

Figure 3 shows raw data of an adsorption experiment employing an amine-terminated gold surface and negatively charged aggregates of TiO_2 NCs. During the course of adsorption, all values steadily increases in magnitude. At $t = 90$ min adsorption was stopped. Figure 4a shows time-averaged values from Figure 3 for $t > 90$ min versus overtone order n (that is, versus the operating frequency of the crystal). Clearly, there is a coupled resonance. Δf is negative at $n = 1$ (eq 3) and positive at $n > 3$ (eq 4). At the crossover, the bandwidth shows a pronounced maximum. Equation 4 applies to the limit of strictly elastic coupling. In this regime, the frequency should decrease with overtone order n. The data shown in Figure 4 do not quite reach this range at high n. Δf is positive, but the coupled resonance is so broad that Δf still increases with n. Figure 4b shows analogous data for adsorption of positively charged (PAH-terminated) TiO_2 NCs to a negatively charged surface. The phenomenology is similar.

Figure 5 shows data from the second set of experiments. Displayed are real-time frequency shift data resulting from 2.8 μm diameter streptavidin-coated beads binding to a QCM surface coated with either control antibodies or specific biotinylated antibodies. Consider the 2.8 μm bead data first (Figure 5a). Before the large magnetic particles bind, the sensor responds to adsorption of the small molecules with a negative frequency change of approximately 300 Hz. At $t = 1600$ s, the magnetic beads are injected and the sensor responds with a strong positive frequency change; over 1 kHz of positive frequency shift is observed in one experiment. Examining the 1.0 μm bead data (Figure 5b), the same negative frequency change is observed when the antibodies bind to the sensor surface. When the beads are injected at $t = 1500$ s, the frequency change is again seen to be positive. Compared to the 2.8 μm beads, the response is rather smaller with typically 200 Hz of positive frequency change measured during the bead injection.

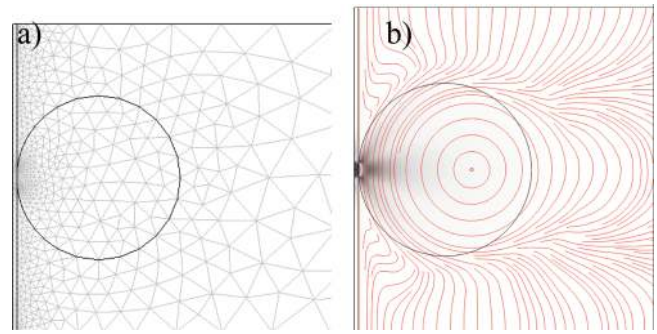

Figure 6. Images from the finite element modeling (FEM) calculation, which reproduces the experimental findings from Figure 4a: (a) geometry and mesh and (b) stream lines and magnitude internal stress. The gray scale and the numerical values of the speed are of little practical relevance because they scale with the driving voltage.

Finite Element Modeling. In order to further substantiate our interpretation of positive frequency shifts in terms of the coupled resonance model, we have performed finite element method (FEM) calculations. The methodology of these calculations has been described in detail in refs 31 and 32. The calculations rely on the small-load approximation[28,33]

$$\frac{\Delta f^*}{f_F} \approx \frac{i}{\pi}\frac{Z_L}{Z_q} = \frac{i}{\pi Z_q}\langle \sigma / \dot{u} \rangle_{area} \qquad (5)$$

$Z_L = \sigma/\dot{u}$ is the "load impedance, σ is the tangential stress at the crystal surface, $\dot{u}$ is the lateral speed at the crystal surface, and angled brackets ($\langle\ \rangle$) denote an average. The flow field around a sphere (more precisely, around a cylinder; the model only captures a 2D geometry) adsorbed to the oscillating surface is readily calculated with commercial software packages. We employed the Incompressible Navier Stokes Module of COMSOL's Multiphysics package (COMSOL GmbH, Göttingen, Germany). Figure 6a shows the geometry and the mesh. The crystal surface is located on the left-hand side. It oscillates tangentially with an amplitude of 0.01 nm. Periodic boundary conditions are applied at the top and at the bottom. Neutral boundary conditions are applied at the right-hand side of the cell.

(31) Rojas, E.; Gallego, M.; Reviakine, I. *Anal. Chem.* **2008**, *80*, 8982.
(32) Johannsmann, D, Reviakine, I.; Richter R. P. Submitted.
(33) Eggers, F.; Funck, T. *J. Phys. E—Sci. Instrum.* **1987**, *20*, 523.

On the right-hand side, the cell extends much beyond the range displayed. The cell is 10 μm wide and 3 μm high. The diameter of the adsorbed sphere is 1.6 μm.

The liquid was modeled as water with a viscosity of $\eta = 1$ mPa s. The stiffness of the sphere was variable. Its loss tangent was tan $\delta = 0.158$ in all cases. Its shear modulus at 5 MHz, $|G|$, was varied between 3 and 300 MPa. Since most materials show viscoelastic dispersion in the MHz range, we assumed $|G|$ to scale as n, where n is the overtone order. The minimum mesh size was chosen as 50 nm close to the three-phase line in order to account for singularity in stress occurring at the three-phase line. Otherwise, the default meshing was employed. In order to calculate the complex frequency shift, one needs to average the tangential stress over the left cell boundary (that is, the crystal surface) and to insert this stress into eq 5.

Figure 6b displays the lines of flow and the magnitude of the local shear stress ($\eta|dv_x/dy + dv_y/dx|$). The overtone order was $n = 1$ in this case. The sphere's modulus at 5 MHz was $|G| =$ 300 MPa, that is, the sphere was "hard". There is an evanescent shear wave on the left-hand side of the cell. The sphere moves with the crystal surface at the point of contact. The fluid on the right-hand side is quiescent. The values of stresses and speeds scale with the drive level. Generally speaking, the stresses are well below 1 MPa unless very peculiar conditions are chosen. Rupture in the sense of rupture event scanning[34] requires extremely high drive levels.

There is somewhat of a conceptual difference between eq 2 (which is based on discrete elements like a sphere and a spring) and the FEM model (which is based on continuum mechanics). One could, in principle, try to extract an equivalent mass and an equivalent contact stiffness from FEM calculations. At this point, we leave it with a qualitative argument. By making the sphere stiffer, we increase the contact stiffness, thereby increasing ω_S.

Figure 7 displays the central outcome of these calculations in the form of a plot of Δf and $\Delta\Gamma$ versus overtone order, n. Different lines correspond to different moduli of the sphere. Since the geometry does not have a link explicitly included, the stiffness of the sphere sets the stiffness of the contact zone, which acts as the link. Varying the stiffness of the sphere (and the stiffness of the link), we vary the parameter ω_S in eqs 2 and 3. The mass of the particle remains unchanged (where, strictly speaking, the "effective mass" includes some comoving solvent).

All values shown in Figure 7 are much larger than in experiment (Figure 4) because the coverage in the simulation is above 50%, whereas it is in the 1% range in experiment (cf. Figure 2). Coverage in the simulation is the ratio between the diameter of the sphere and the cell size. Simulating small coverages requires the use of large cells, which is computationally demanding.

In the limit of a stiff sphere ($|G| = 300$ MPa, diamonds), the sphere moves (almost) rigidly with the crystal. As a consequence, Δf is negative. The situation corresponds to "inertial loading" in Figure 1. For the soft spheres ($|G| = 30$ MPa and softer), Δf is positive. The contact between the sphere and plate is so compliant that the spheres do not move appreciable. This situation corresponds to "elastic loading" in Figure 1. Interestingly, there is an intermediate situation ($|G| = 100$ MPa, lower triangles), where the behavior changes over from inertial loading at low overtone orders to elastic loading at high overtone orders. This data set should be compared to Figure 4. Under certain circumstances, the coupled resonance predicted by Dybwad is right in the accessible window of frequencies. These conditions were matched in the experiments shown in Figures 3 and 4 and they are matched in the simulation for $|G| = 100$ MPa. This proves the presence of the coupled resonance. The evidence is less direct for the example shown in Figure 5. Still, it is fair to assume that the reason behind the positive frequency shifts is given by point contacts, as well.

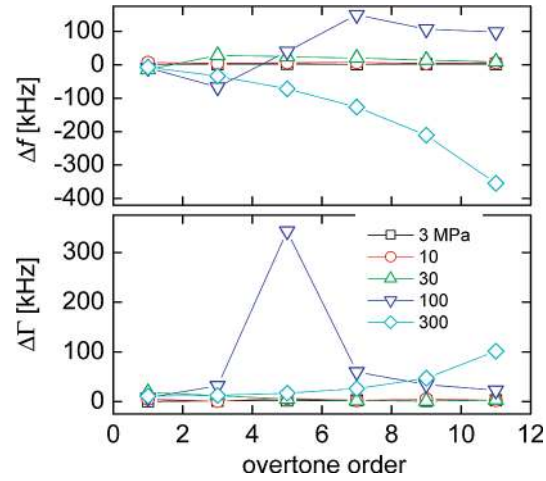

Figure 7. Shifts of frequency and bandwidth versus overtone order for five different stiffnesses of the sphere, as obtained with the FEM calculation. Of particular interest is the case of stiffness 100 MPa on the fundamental. One observes a coupled resonance, reproducing the data from Figure 4a. Stiffer spheres behave as inertial loads, softer spheres behave as elastic loads (cf. Figure 1).

CONCLUSIONS

Adsorbing large diameter (>1 μm) colloidal objects to the surface of a quartz crystal microbalance, one can observe *positive* frequency shifts. As evidenced by a finite element calculation, these most likely arise from point contacts between the adsorbate particles and the sensor surface. The general phenomenology is similar to spheres in air, even though liquid leads to a strong coupling between the sphere and the plate. For such situations, the frequency shift depends on the *stiffness of the contact*, rather than the size of the adsorbed object.

ACKNOWLEDGMENT

M.C. and R.H. acknowledge the support of the UK Technology Strategy Board Micro & Nanotechnology Award 0231: "Acoustic microsensors for healthcare and environmental monitoring". A.P., G.G., and D.S. acknowledge support by the VW-Stiftung.

Received for review September 7, 2009. Accepted February 9, 2010.

AC902012E

(34) Cooper, M. A.; Dultsev, F. N.; Minson, T.; Ostanin, V. P.; Abell, C.; Klenerman, D. *Nat. Biotechnol.* **2001**, *19*, 833–837.